Supporting Information

In situ surface-trap passivation of $CuBi_2O_4$ photocathodes for unbiased solar water splitting

Yingfei Hu,[ab] Jun Wang,[a] Huiting Huang,[ac] Jianyong Feng,*[ac] Wangxi Liu,[a] Hangmin Guan,[b] Lingyun Hao,[b] Zhaosheng Li ,*[ac] and Zhigang Zou[a]

[a]Collaborative Innovation Center of Advanced Microstructures, National Laboratory of Solid State Microstructures, School of Physics, Nanjing University, 22 Hankou Road, Nanjing 210093, China

[b]School of Materials Engineering, Jinling Institute of Technology, 99 Hongjing Avenue, Nanjing 211169, China

[c]College of Engineering and Applied Sciences, Nanjing University, Nanjing 210093, China

Corresponding author. E-mail: fengjianyong@nju.edu.cn (Jianyong Feng)
Corresponding author. E-mail: zsli@nju.edu.cn (Zhaosheng Li)

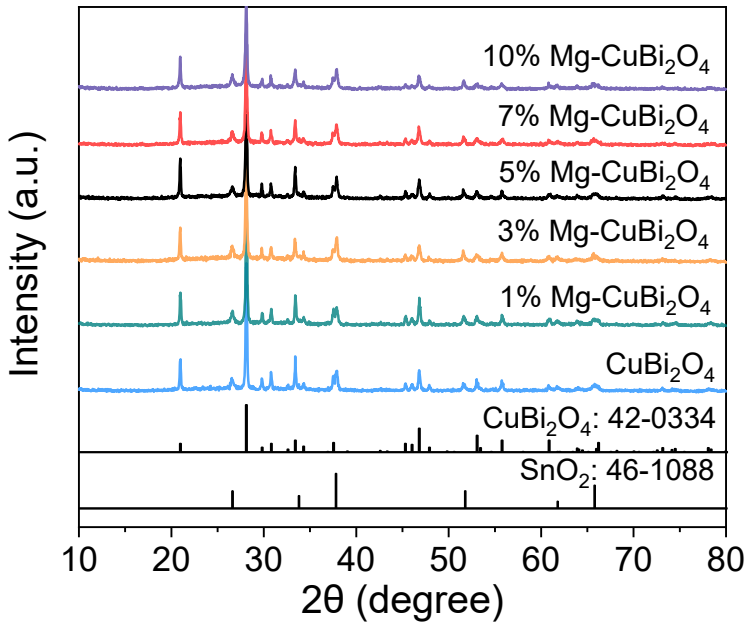

Figure S1. XRD patterns of $CuBi_2O_4$ films with different amounts of Mg (0, 1%, 3%, 5%, 7%, 10%).

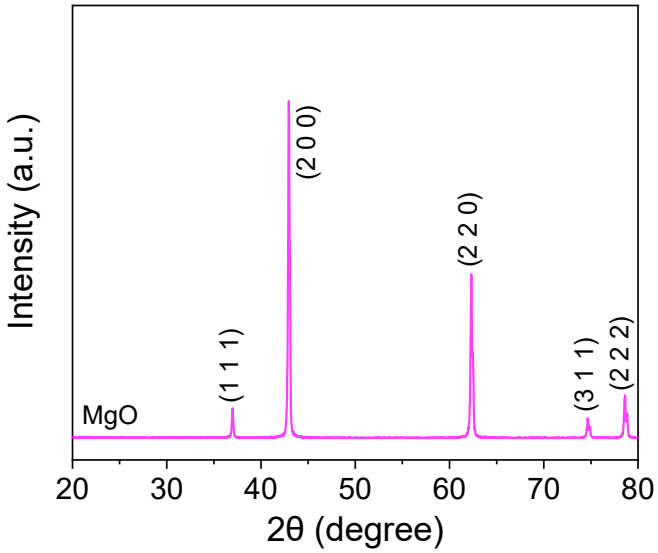

Figure S2. XRD pattern of MgO prepared by directly calcination of the magnesium precursor.

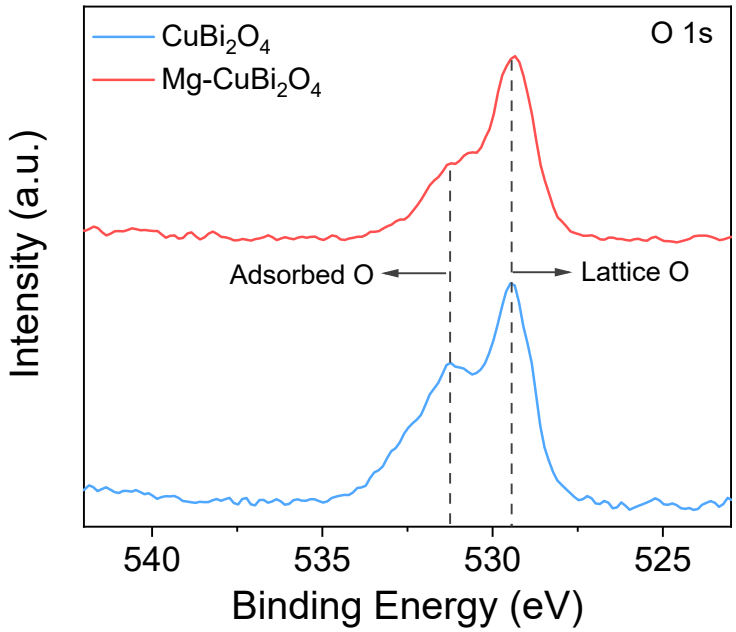

Figure S3. XPS spectra of O 1s orbits in $CuBi_2O_4$ and Mg-$CuBi_2O_4$ samples.

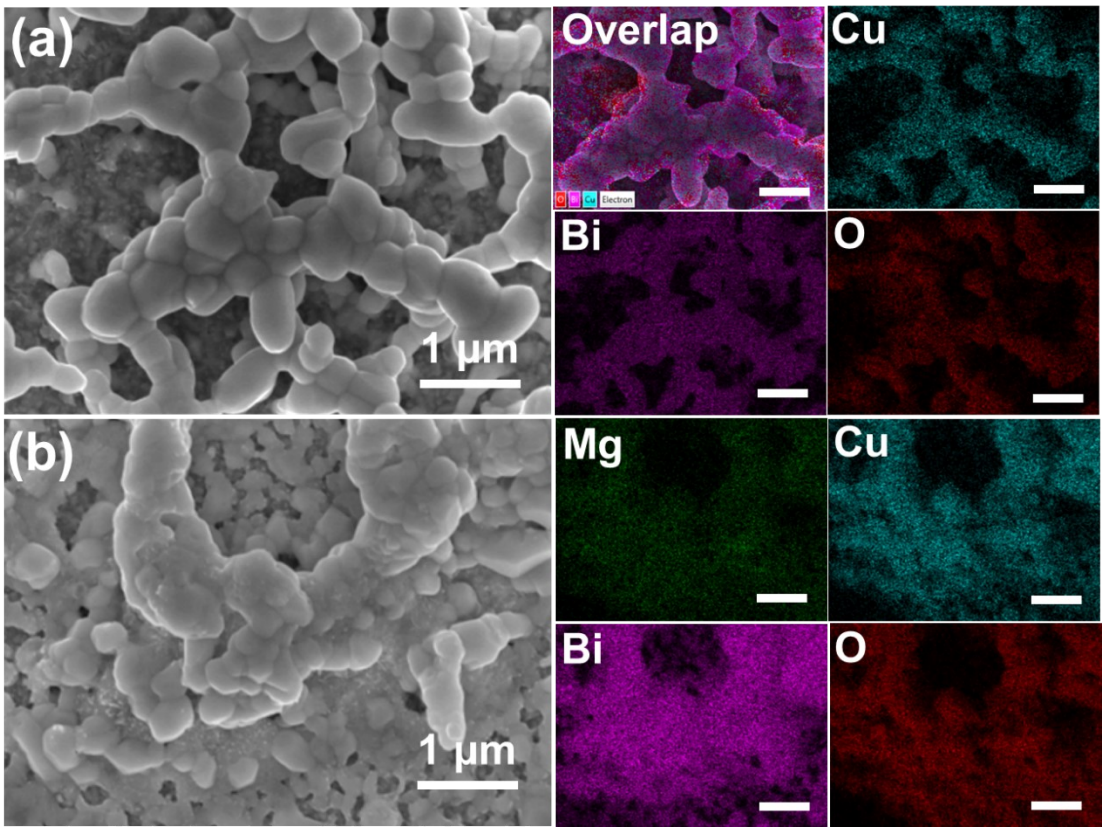

Figure S4. SEM images of (a) $CuBi_2O_4$, (b) Mg-$CuBi_2O_4$ Films and EDS elemental mappings of the Mg-$CuBi_2O_4$ sample.

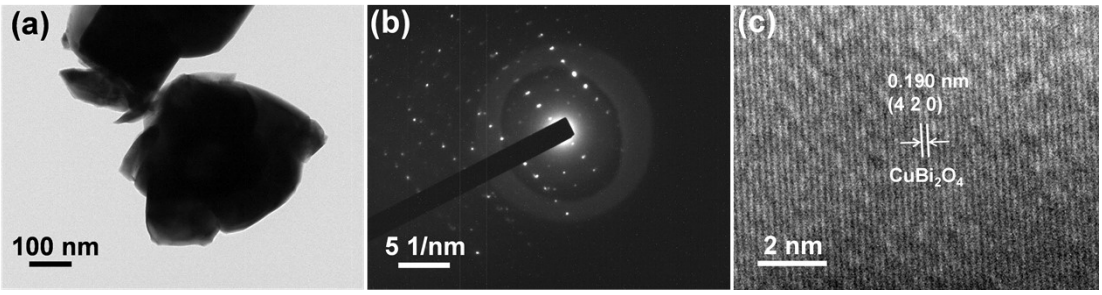

Figure S5. (a) TEM, (b) SAED, and (c) HR-TEM images of $CuBi_2O_4$.

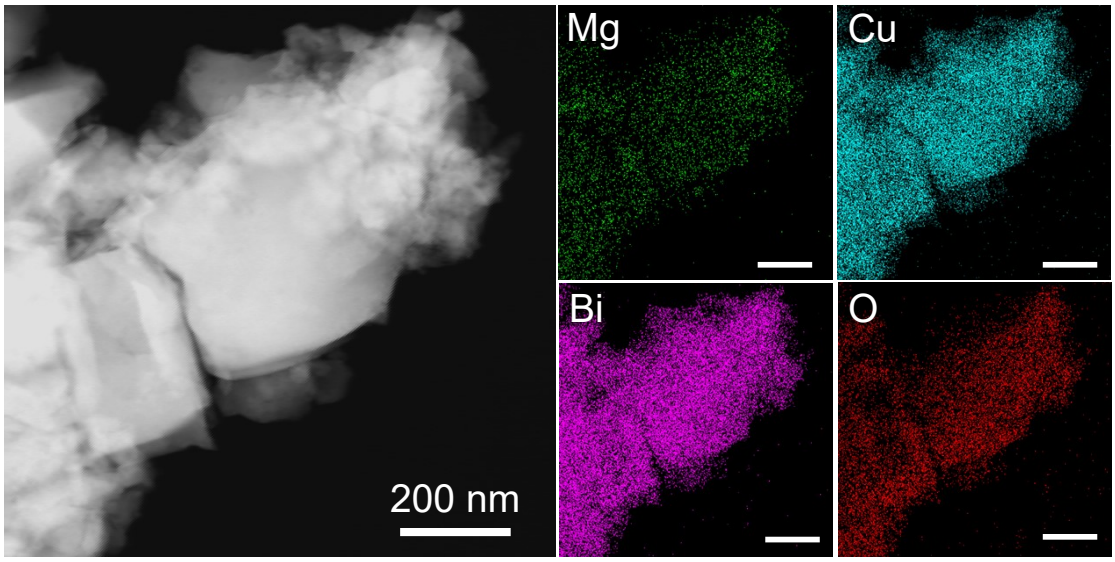

Figure S6. TEM image and EDS elemental mappings of the Mg-$CuBi_2O_4$ sample (scale bar: 200 nm)

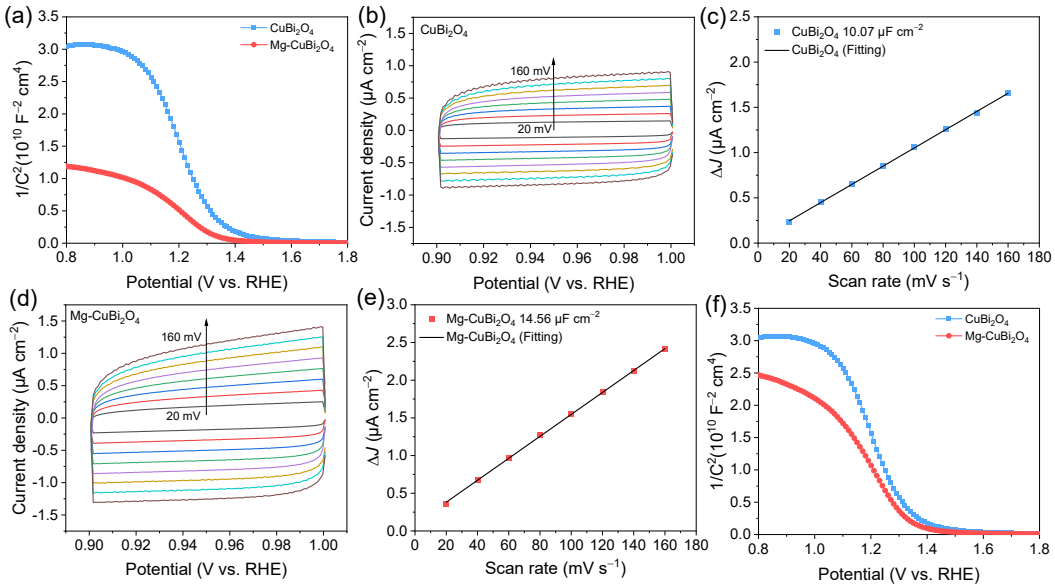

Figure S7. (a) Mott–Schottky plots of $CuBi_2O_4$ and Mg-$CuBi_2O_4$ photocathodes. Electrochemically active surface areas (ECSA) measurements: cyclic voltammetry (CV) curves of (b) $CuBi_2O_4$ and (d) Mg-$CuBi_2O_4$ photocathodes by various scan rates (20–160 mV/s); double-layer capacitance (C_{dl}) of (c) $CuBi_2O_4$ and (e) Mg-$CuBi_2O_4$depended by the difference between J_a and J_c values. (f) Mott–Schottky plots which have been corrected with ECSA data.

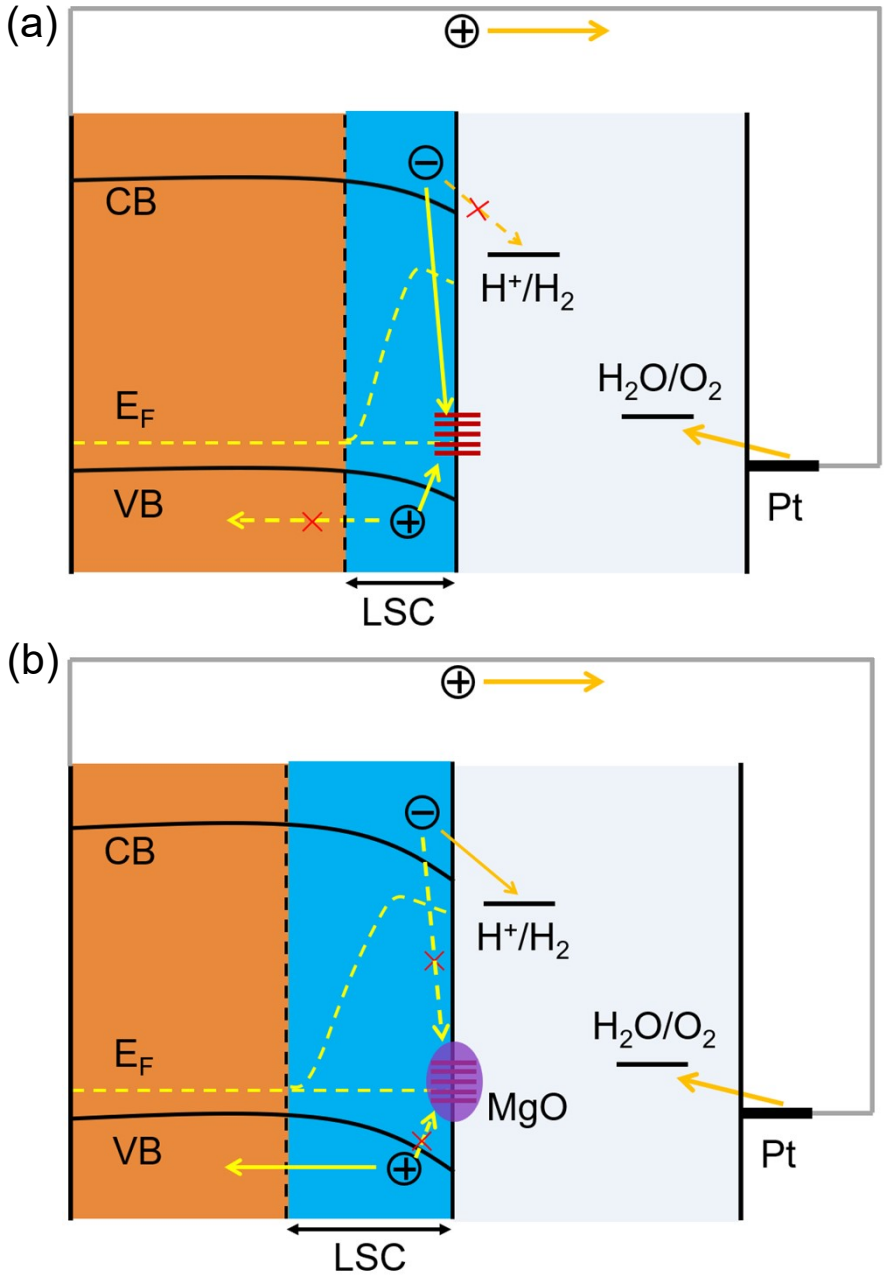

Figure S8. Schematic diagrams of the energy band of $CuBi_2O_4$ photocathodes: (a) bare $CuBi_2O_4$; (b) Mg-$CuBi_2O_4$.

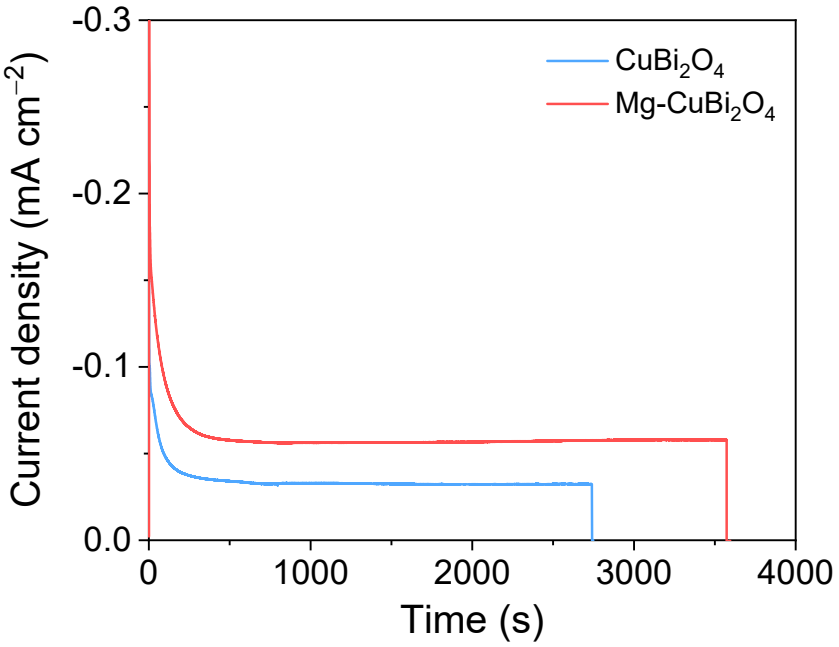

Figure S9. I–t curves of $CuBi_2O_4$ and Mg-$CuBi_2O_4$ photocathodes.

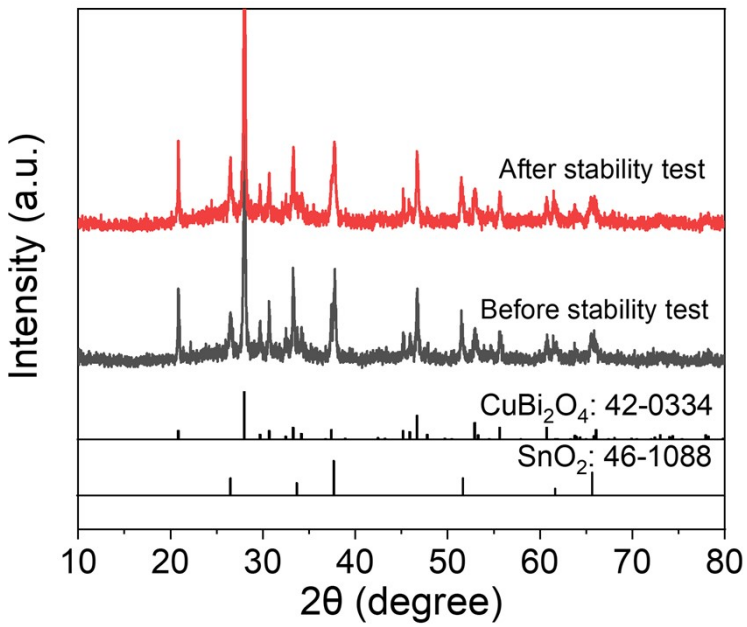

Figure S10. XRD patterns of Mg-$CuBi_2O_4$ photocathode before and after stability test.

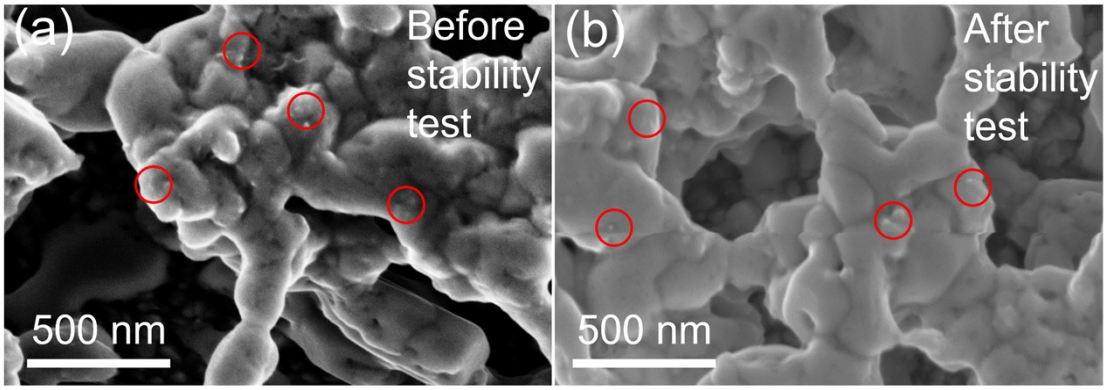

Figure S11. SEM images of Mg-$CuBi_2O_4$ photocathode before and after stability test. (Several MgO particles are marked by red circles.)

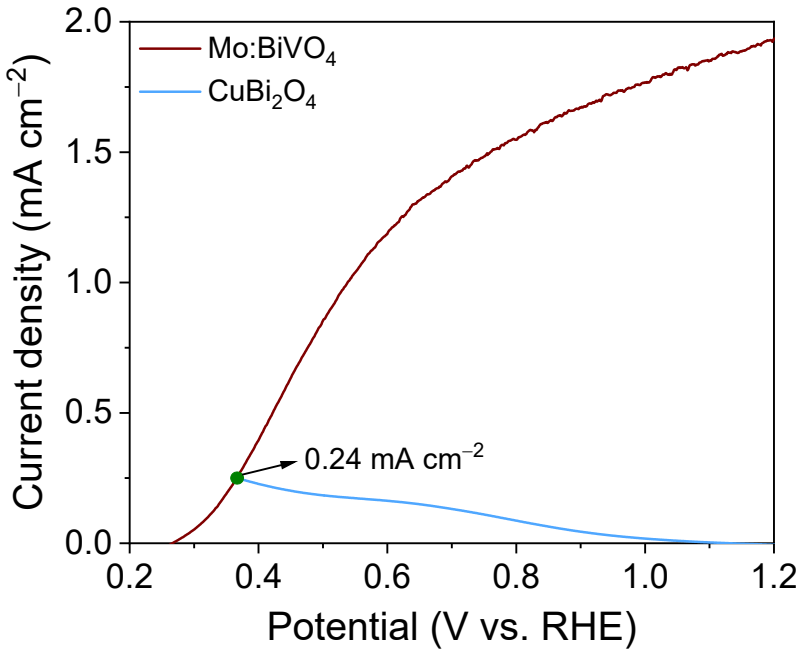

Figure S12. *J*–V curves of a single Mo:$BiVO_4$ photoanode and a single $CuBi_2O_4$ photocathode.

Table S1. Summary of various $CuBi_2O_4$ photocathodes for PEC water reduction.

Photocathode structure	Electrolyte	Onset potential	Photocurrent	Ref.
FTO/$CuBi_2O_4$/TiO_2/Pt	0.1 M NaOH	1.2 V_{RHE}	–0.35 mA·cm^{-2} at 0.6 V_{RHE}	1
FTO/Ag- $CuBi_2O_4$ SMRs/NGQDs	0.5 M Na_2SO_4; pH=6.6	1.05 V_{RHE}	–0.071 mA·cm^{-2} at 0.3 V_{RHE}	2
FTO/$CuBi_2O_4$ (Rapid thermal processing)	0.3 M K_2SO_4/0.2 M phosphate buffer solution; pH=7	1.2 V_{RHE}	–0.38 mA·cm^{-2} at 0.6 V_{RHE} (with H_2O_2)	3
FTO/O_v/$CuBi_2O_4$/Zn-$CuBi_2O_4$	0.3 M K_2SO_4/0.2 M phosphate buffer solution; pH=6.65	1.0 V_{RHE}	–0.6 mA·cm^{-2} at 0.3 V_{RHE}	4
FTO/CuO/$CuBi_2O_4$	0.5 M Na_2SO_4; pH = 7	1.0 V_{RHE}	–0.9 mA·cm^{-2} at 0.1 V_{RHE}	5
FTO/CuO/$CuBi_2O_4$	0.1 M NaOH ; pH=13	1.12 V_{RHE}	–1.49 mA·cm^{-2} at 0.6 V_{SHE}	6
FTO/$CuBi_2O_4$/Pt	0.2 M K_2HPO_4/0.2 M KH_2PO_4/0.3 M K_2SO_4	1.0 V_{RHE}	–0.5 mA·cm^{-2} at 0.4 V_{RHE}	7
FTO/nano$CuBi_2O_4$	0.1 M NaOH	1.05 V_{SHE}	–0.23 mA·cm^{-2} at 0.4 V_{SHE}	8
FTO/Mg-$CuBi_2O_4$	KB_i (KOH: 0.2 M; H_3BO_3: 0.4 M); pH=9.2	1.15 V_{RHE}	–0.2 mA·cm^{-2} at 0.7 V_{RHE}	This work

Table S2. Comparison of $CuBi_2O_4$ and other photocathodes for PEC water reduction.

Photocathode structure	Electrolyte	Onset potential	Photocurrent	Ref.
MoS_2-n^+p Si	0.5 M H_2SO_4; pH=0	0.35 V_{RHE}	–17 mA·cm^{-2} at 0 V_{RHE}	9
FTO/Cu_2O/Ga_2O_3 /TiO_2/RuO_x	0.5 M Na_2SO_4/0.2 M phosphate solution; pH=5	1.0 V_{RHE}	–10 mA·cm^{-2} at 0 V_{RHE}	10
FTO/CuO/Pd	0.2 M $H_2BO_3^-$/H_3BO_3; pH=9.2	0.1 V_{SCE}	–0.8 mA·cm^{-2} at –0.3 V_{SCE}	11
Mo glas/Cu_2ZnSnS_4 /CdS/In_2S_3/Pt	0.2 M Na_2HPO_4/ NaH_2PO_4; pH=6.5	0.8 V_{RHE}	–11.1 mA·cm^{-2} at 0 V_{RHE}	12
FTO/$CuFeO_2$	1 M NaOH; pH=13.5	0.98 V_{RHE}	–0.9 mA·cm^{-2} at 0.4 V_{RHE}	13
FTO/Mg-$CuBi_2O_4$	KB_i (KOH: 0.2 M; H_3BO_3: 0.4 M); pH=9.2	1.15 V_{RHE}	–0.2 mA·cm^{-2} at 0.7 V_{RHE}	This work

References

1. X. Zhu, Z. Guan, P. Wang, Q. Zhang, Y. Dai, B. Huang, *Chinese J. Catal.*, 2018, **39**, 1704-1710.
2. C. Ma, D. -K. Ma, W. Yu, W. Chen, S. Huang, *Appl. Surf. Sci.*, 2019, **481**, 661-668.
3. R. Gottesman, I. Levine, M. Schleuning, R. Irani, D. Abou-Ras, T. Dittrich, D. Friedrich, R. Krol, *Adv. Energy Mater.*, 2021, **11**, 2003474.
4. S. Wei, C. Wang, X. Long, T. Wang, P. Wang, M. Zhang, S. Li, J. Ma, J. Jin, L. Wu, *Nanoscale*, 2020, **12**, 15193-15200.
5. S. Pulipaka, N. Boni, G. Ummethala, P. Meduri, *J. Catal.*, 2020, **387**, 17-27.
6. S. A. Monny, L. Zhang, Z. Wang, B. Luo, M. Konarova, A. Du, L. Wang, *J. Mater. Chem. A*, 2020, **8**, 2498-2504.
7. S. P. Berglund, F. F. Abdi, P. Bogdanoff, A. Chemseddine, D. Friedrich, R. van de Krol, *Chem. Mater.*, 2016, **28**, 4231-4242.
8. C. -Y. Lin, S. -Y. Lin, M. -C. Tsai, C. -H. Wu, *Sustain. Energy Fuels*, 2020, **4**, 625-632.
9. J. D. Benck, S. C. Lee, K. D. Fong, J. Kibsgaard, R. Sinclair, T.F. Jaramillo, *Adv. Energy Mater.*, 2014, **4**, 1400739.
10. L. Pan, J. H. Kim, M. T. Mayer, M. -K. Son, A. Ummadisingu, J.S. Lee, A. Hagfeldt, J. Luo, M. Grätzel, *Nat. Catal.*, 2018, **1**, 412-420.
11. X. Guo, P. Diao, D. Xu, S. Huang, Y. Yang, T. Jin, Q. Wu, M. Xiang, M. Zhang, *Int. J. Hydrogen Energy*, 2014, **39**, 7686-7696.
12. X. Wen, W. Luo, Z. Guan, W. Huang, Z. Zou, *Nano Energy*, 2017, **41**, 18-26.
13. C. G. Read, Y. Park, K. S. Choi, *J. Phys. Chem. Lett.*, 2012, **3**, 1872-1876.